JOURNAL OF CATALYSIS 155, 204–218 (1995)

Structure Sensitive Selectivity of the NO–CO Reaction over Rh(110) and Rh(111)

Charles H. F. Peden, David N. Belton,* and Steven J. Schmieg*

*Environmental Molecular Sciences Laboratory, Pacific Northwest Laboratory,[1] P.O. Box 999, Richland, Washington 99352; and *Physical Chemistry Department, General Motors Research and Development Center, 30500 Mound Road, Box 9055, Warren, Michigan 48090-9055*

Received May 23, 1994; revised March 14, 1995

We have studied the effects of temperature, NO conversion, and NO–CO ratio on the activity and selectivity of the NO–CO reaction at high (1 Torr $< P <$ 100 Torr) pressures over the Rh(110) and Rh(111) surfaces. Under the conditions used in this study, the NO–CO activity, as measured by the rate of NO loss, is between 1.3 and 6.3 times faster over Rh(110) than over Rh(111). The (110) surface exhibits a lower apparent activation energy (E_a), 27.2 vs 34.8 kcal/mol, than does the (111) surface. We attribute this behavior to a slightly more facile NO dissociation process on the more open (110) surface. Although the turnover numbers for NO reaction can be quite similar on the two different surfaces, we find large differences between Rh(110) and Rh(111) with regard to their selectivities for the two competitive nitrogen-containing products, N_2O vs N_2. The more open Rh(110) surface tends to make significantly less N_2O than Rh(111) under virtually all conditions that we probed with these experiments. This can be understood in terms of the relative surface coverages of adsorbed NO and N atoms on the two surfaces. Notably, more facile NO dissociation on Rh(110) appears to lead to greater steady-state concentrations of adsorbed N atoms than is present on the (111) surface. Higher N atom coverages on the (110) surface favor N atom recombination (N_2 formation) more than the NO + N reaction (N_2O formation) on Rh(110) relative to Rh(111). Indeed, Rh(110) surfaces were found to be largely composed of adsorbed N atoms and lesser quantities of NO in postreaction XPS measurements. In contrast, Rh(111) surfaces showed only X-ray photoelectron spectroscopy features due to adsorbed NO.

I. INTRODUCTION

Automotive emissions of nitrogen oxides (NO_x) are very effectively controlled in U.S. passenger cars by a heavy reliance on aftertreatment of the engine exhaust using catalytic converters that contain a mixture of platinum (Pt), rhodium (Rh), and sometimes palladium (Pd) (1, 2). Both Pt and Rh are very effective at oxidizing CO to CO_2, but it is generally believed that Pt and Pd are superior for hydrocarbon (HC) oxidation with Rh being best for NO reduction. Beginning in 1994, new government regulations will take effect which mandate that NO_x emissions from passenger cars must fall substantially from their 1993 levels of 1.0 g/mile to as low as 0.2 g/mile (2, 3). Considering that under warmed-up conditions the current generation of emission control technology already removes over 80% of the NO_x from the exhaust stream, the 0.2 g/mile standard will require improving the warmed-up efficiency of the NO_x reduction process to over 95%. These tougher U.S. standards will take effect at the same time that most European countries are adopting regulations which will effectively double the number of vehicles worldwide that are equipped with a catalytic converter. Given these strong pressures on noble metal supply, it is imperative that Rh and Pt be utilized as effectively as possible for the control of automotive emissions; one part of our effort is focused on obtaining a more detailed understanding of the reactivity of these vital catalyst components. To this end we have a continuing program to define and understand the reaction kinetics over well defined single crystal catalysts under conditions of temperature and pressure comparable to those encountered in automotive exhaust. By studying such well defined model catalysts, we are able to isolate the activity of the noble metal component of the catalyst free from complicating factors such as metal particle size and catalyst support effects. Because single crystals have well-defined surface structures, surface areas, and no support effects, they are ideal for activity comparisons between metal surfaces with varying geometric structures.

In this paper we examine the effect of surface structure on the NO–CO activity and selectivity by comparing the reactivity of Rh(110) and Rh(111) single crystal catalysts. Selectivity for the two possible nitrogen-containing products from NO reduction, N_2O and N_2, is particularly interesting. Notably, the present work was motivated by recent results that suggested that the selectivity for N_2O

[1] Pacific Northwest Laboratory is a multiprogram national laboratory operated for the U.S. Department of Energy by Battelle Memorial Institute under Contract DE-AC06-76RLO 1830.

0021-9517/95 $12.00

over (111) surfaces of Rh (4) and Pt–Rh (5) single crystal catalysts is dominated by steric crowding of adsorbed NO. We suspected that this crowding inhibited the NO dissociation reaction, leading to high steady-state surface coverages of NO, correspondingly low N atom coverages, and, thus, relatively high selectivity toward N_2O production over that of N_2. Within this model we reasoned that a more open surface like Rh(110) might not allow NO to pack as tightly on the surface, thereby resulting in more favorable conditions for N_2 formation and less N_2O production. Furthermore, it is generally believed that surface atoms with a lower coordination number, such as those found on fcc(110) surfaces, are more active for the dissociation of small molecules (6). This is apparently the case for NO dissociation on Rh (7–9). Previous experiments comparing the CO_2 formation rates from the NO–CO reaction over Rh(111) and Rh(100) had suggested that this reaction was structure sensitive (10). Therefore, there was ample reason to believe that the reactivity of the (110) surface should differ from that of Rh(111). A second motivation for this work was to assess what role surface structure might play in determining the selectivity of supported Rh catalysts. Previous papers describing studies of supported Rh catalysts show some notable differences in the temperature dependence of N_2O selectivity. Over 4.6 wt% Rh/silica (SiO_2), it was reported that N_2O is the major product over a fairly wide range of reaction temperatures and NO conversions (11). This result was quite similar to recent results obtained over Rh(111) (4). In contrast, low-loaded Rh/alumina (Al_2O_3) catalysts have been shown to more readily switch from making primarily N_2O at low temperatures and NO conversions to making primarily N_2 at higher temperatures (12–17). Considering the very different loadings present in these two types of catalysts, we suspected that particle size-dependent structural changes may play an important role in determining the selectivity of these catalysts. Since the effect of surface structure on the N_2O selectivity had not been previously examined, we felt that such a study could make an important contribution to our understanding of NO reduction reactions over Rh catalysts.

Numerous studies have been published on the NO–CO reaction at pressures around 10 Torr over supported Rh (11–17), and Rh single crystal (4, 10, 18) catalysts. While there were a few discrepancies in some of the earlier studies of single crystal Rh (10, 18), there is now general agreement as to the kinetics and selectivities at low temperature and/or low NO conversion for both single crystal (4) and supported (11–17) Rh. Over all of these catalysts, it is reported that N_2O is the primary N-containing product, the apparent activation energy (above 480 K) is between 33 and 38 kcal/mol, and the reaction rate and selectivity are roughly independent of both the CO and NO pressures (between 1 and 100 Torr). However, the behavior of these various catalysts are significantly different at higher temperatures and/or NO conversions. Whereas Rh(111) (4) and 5 wt% Rh/SiO_2 (11) make less N_2O at high temperature than at lower temperature, N_2O remains the primary product. On the other hand, Rh/Al_2O_3 catalysts produced almost exclusively N_2 at high temperatures and NO conversions (12–17). In contrast to the results just described that were obtained at moderate pressures, studies of the NO–CO reaction over polycrystalline and single crystal Rh at total pressures below 10^{-4} Torr have observed little, if any, N_2O as a reaction product (19–22).

The results reported in this paper demonstrate that the selectivity of the NO–CO reaction is quite sensitive to the structure of the Rh catalyst metal surface. Notably, the more open Rh(110) surface tends to make significantly less N_2O than Rh(111) under virtually all conditions that we probed with these experiments. In particular, at the highest temperatures and NO conversion levels studied here, we found that Rh(110) produced almost entirely N_2, while on Rh(111) the N_2O selectivity was never less than 40%. Furthermore, under the conditions used in this study, the NO–CO activity over Rh(110), as measured by the rate of NO loss, is somewhat faster than over Rh(111) with a lower apparent activation energy (E_a), 27.6 vs 35.4 kcal/mol. We attribute these results to the greater tendancy of the more open (110) surface to dissociate NO. Notably, more facile NO dissociation on Rh(110) would lead to greater steady-state concentrations of adsorbed N atoms; thus, the (110) surface favors N atom recombination over the surface reaction between adsorbed NO and N atoms to make N_2O. In support of this, postreaction surface analysis shows only NO on the Rh(111) surface while the Rh(110) surface contains predominantly N atoms and much lower concentrations of adsorbed NO. NO dissociation on Rh(110) is more favorable than on Rh(111), in part, because it is less severely poisoned by high surface concentrations of NO. In addition, the more open (110) surface may be intrinsically more active for the elementary process of dissociating adsorbed NO.

II. EXPERIMENTAL

2.1. Apparatus

The experiments were performed in a custom-built system which couples an ultrahigh vacuum (UHV) analysis chamber to a moderate pressure (<100 Torr) reactor. The reactor and analysis chamber are separated with a gate valve. The UHV analysis chamber is equipped with a wide array of analytical techniques. For this study we used Auger electron spectroscopy (AES), X-ray photoelectron spectroscopy (XPS), and low energy electron diffraction (LEED). The gases used in these experiments were 99.0% NO and 99.99% CO (Scott Specialty Gases). The NO had <0.35% N_2O and <0.5% N_2 contamination,

while the CO was in an Al cylinder and was trapped with a liquid nitrogen bath to exclude any metal carbonyls from the reactor. The gases were leaked into the reactor at low pressure as measured by a baratron gauge. The reactor has a volume of 0.673 liters and is pumped with a turbomolecular pump with an ultimate base pressure of 10^{-9} Torr. The pump is separated from the reactor with a gate valve. The sample could be transferred from the reactor to the UHV analysis chamber within 5 min after reactor pumpdown with a typical base pressure of 10^{-9} Torr during spectroscopic analysis.

2.2. Sample Preparation

The Rh(110) and Rh(111) samples were obtained from a boule of Rh oriented along the [100] direction. Both crystals were cut so that both sides of each sample were oriented to ±0.5° of the (110) and (111) planes as shown by the Laue diffraction patterns. The initial cleaning procedure consisted of flowing 99.9999% H_2 at 50 sccm over the samples in a quartz tube furnace for 36 h at 1275 K. This procedure has been shown to be effective at removing any low Z impurities from the bulk, such as C, B, P, and Si (23). The samples were then sanded and polished with diamond paste with the final polish utilizing 0.25-μm grit. After polishing, each crystal was etched in hot HF/HNO_3 (3/1) for several minutes. The Rh(110) sample was examined first, followed by the Rh(111) sample. A crystal was mounted on the transfer device using two etched 0.015-inch Ta wires spot welded to the edges of the sample for resistive heating. A 0.003-inch chromel–alumel thermocouple was also spot welded to the edge of the sample to monitor the crystal temperature. After mounting, the sample was rinsed again with HNO_3 to remove spot welding residue, followed by rinsing with distilled H_2O and methanol. The Rh(110) sample was rectangular in shape (8.03 × 4.95 mm) with an area of 0.398 cm^2 per side and a thickness of 0.94 mm. The number of active sites was calculated to be 1.58×10^{15} (both sides), and for this calculation the atoms in the troughs are included. The Rh(111) sample was rectangular in shape (8.69 × 6.02 mm) with an area of 0.523 cm^2 per side and a thickness of 0.91 mm. The number of active sites was calculated to be 1.67×10^{15} (both sides), and for this calculation the atoms below the threefold hollow sites are *not* included. The edge areas accounted for approximately 19% of the total area of each sample.

2.3. Sample Cleaning

A sharp (1 × 1) LEED pattern was obtained on the front and back of the Rh(110) sample by Ar^+ sputtering (2 keV, ~12 μA) for ~42 h with the sample at 875 K, followed by annealing at 1275 K for 20 min. A similar procedure was used to order the front and back of the Rh(111) sample. This extensive sputtering treatment was necessary to obtain a sharp LEED pattern and has been successful in ordering Rh single crystal surfaces. Next, the sample was placed in the reactor and treated in an 8-Torr CO/8-Torr O_2 gas mixture at 525 K several times. The surface cleanliness was monitored with AES and XPS and the surface order was checked periodically with LEED.

2.4. Gas Chromatography Measurements

Reactions were performed in a batch mode. All products and reactants were measured with a Varian 3400 gas chromatograph (GC) using simultaneous injection of sample (2 × 250 μl) into each of two columns operated at 313 K with a He carrier gas. One gas sample entered a molecular sieve column where N_2, NO, and CO were separated before passing on to the detectors for analysis. The other sample entered a delay column followed by a Hayesep DIP column which delayed entry and subsequent elution of components until the last molecular sieve component (CO) eluted. At this point a valve was switched to direct the Hayesep DIP effluent to the detectors for the measurement of CO_2 and N_2O. Column effluents were monitored using both a thermal conductivity detector (TCD) and a flame-ionization detector (FID). Gases passed first through the TCD, then through a methanizer with a Ni catalyst, and then to the FID. The TCD filament temperature was maintained at 573 K, the methanizer temperature at 658 K, and the detector temperature at 423 K. Using this arrangement, we were able to detect N_2 (TCD), NO (TCD), CO (FID), CO_2 (TCD), and N_2O (TCD). No other species were monitored because the products, CO_2, N_2 and N_2O, were formed in their expected ratios based on the stoichiometry of the reaction:

$$(1 + x)CO + 2NO \rightarrow xN_2 + (1 - x)N_2O + (1 + x)CO_2 \quad (0 \leq x \leq 1). \qquad [1]$$

The experimental procedure for making a rate measurement was as follows: (i) the gate valves to the UHV analysis chamber and the reactor turbomolecular pump were closed, (ii) the reactants were leaked into the reactor, (iii) the sample was ramped to the reaction temperature at approximately 15 K/s, (iv) the timer was started when the sample was within 5 K of the reaction temperature, (v) the temperature was held (±2 K) for a specified time interval, (vi) the sample was cooled to room temperature, and, finally, (vii) the gases in the reactor were expanded into the evacuated GC sampling loops.

III. RESULTS

3.1. NO–CO Reaction Kinetics

Figure 1 shows the turnover numbers (TONs) for CO_2, N_2O, and N_2 formation obtained on Rh(110) plotted in an

TABLE 1

Apparent Activation Energies and Frequency Factors for CO_2, N_2O, and N_2 from the NO–CO Reaction over Rh(111) and Rh(110) Single Crystal Catalysts

$P_{NO} = P_{CO} = 8$ Torr		CO_2	N_2O	N_2
Rh(111)	E_a[a]	34.2	35.7	32.1
	ν[b]	5.0×10^{13}	1.1×10^{14}	1.6×10^{12}
Rh(110)	E_a[a]	28.0	25.3	29.6
	ν[b]	7.3×10^{11}	3.1×10^{10}	8.3×10^{11}

[a] kcal/mole.
[b] Molecules/site-sec.

Arrhenius fashion as a function of inverse temperature. The data (Fig. 1) were obtained by reacting 8-Torr NO and 8-Torr CO (8/8) over the Rh(110) catalyst. In the temperature range of Fig. 1 (525 K to 675 K), the three products (CO_2, N_2O, and N_2) are formed with apparent activation energies, E_a, of 28.0, 25.3, and 29.8 kcal/mol, respectively, when the data are analyzed using an Arrhenius equation. (Note that this analysis presumes nothing about the mechanism so that we obtain *apparent* activation energies and preexponential factors. However, the TONs are useful for comparison with data obtained on other catalysts.) The corresponding apparent prefactors (ν) are listed along with the activation energies in Table 1. For the experiments in Fig. 1, the data are obtained only over that temperature range for which we could accurately measure TONs—meaning that the total reaction times were greater than 15 s—while keeping the overall NO conversion below 15%. TONs are given on a per-Rh site basis by including both the ridge and trough sites on the surface. By this site accounting method, the number of exposed surface Rh sites is 1.58×10^{15}.

In Fig. 2 we show a direct comparison of the CO_2 TONs for reaction of NO and CO (8/8) over both Rh(110) and Rh(111) along with the N_2 and N_2O TONs for the Rh(111) surface. The number of Rh(111) surface sites is calculated to be 1.67×10^{15} by counting only the atop Rh atoms; Rh atoms below the threefold hollow sites are not included in this case. The two surfaces were studied in the same experimental apparatus within 1 week of each other. Previously, Belton and Schmieg measured the NO–CO reaction rates over Rh(111) in this same apparatus (4). The only difference we observed this time was that all of the TONs were lower (for all three products) by about 35%. (However, the relative error in comparing the present results for Rh(111) and Rh(110) is likely to be less than this.) We consider the two measurements on Rh(111) made 18 months apart to be within the range of experimental error for this experiment. In Table 1, the apparent activation energies and preexponential factors for CO_2,

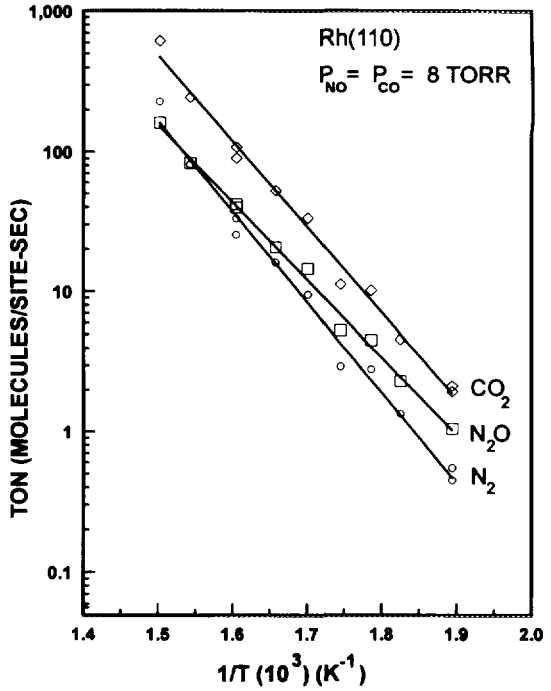

FIG. 1. Specific rates of CO_2, N_2O, and N_2 formation for the NO–CO reaction over Rh(110) as a function of inverse temperature. $P_{NO} = P_{CO} = 8$ Torr.

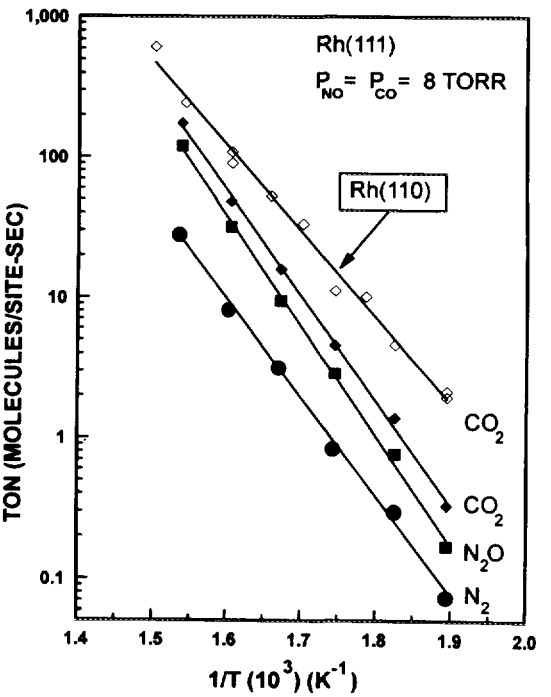

FIG. 2. Specific rates of CO_2, N_2O, and N_2 formation for the NO–CO reaction over Rh(111) as a function of inverse temperature. $P_{NO} = P_{CO} = 8$ Torr. For comparison, also included are the CO_2 formation rates over Rh(110) from Fig. 1.

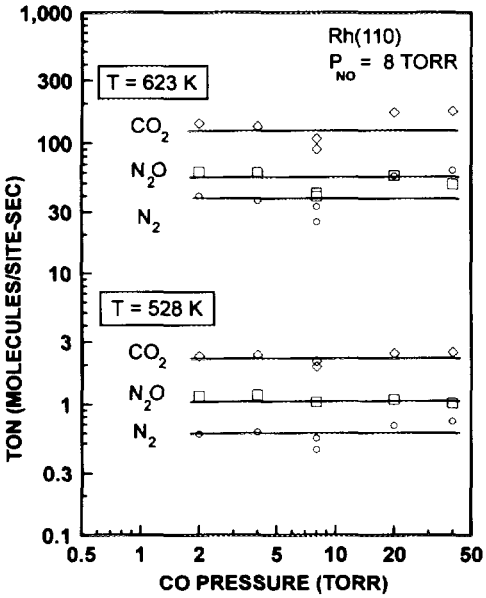

FIG. 3. The CO_2, N_2O, and N_2 TONs as a function of CO pressure with a fixed NO pressure of 8 Torr at 623 K and 528 K over Rh(110). The data show that the production of all three products has an apparent zero-order dependence on CO pressure.

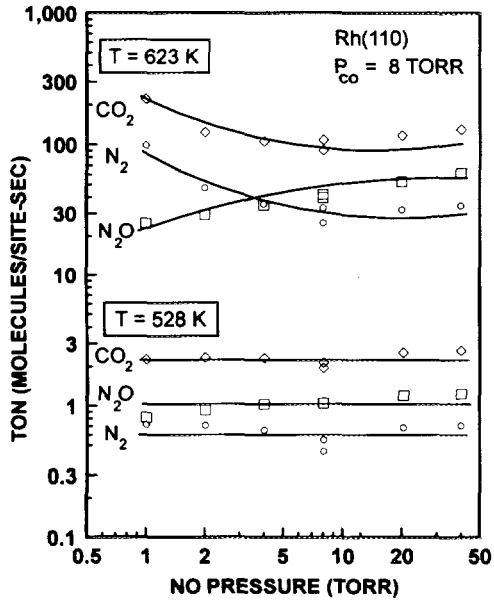

FIG. 4. The CO_2, N_2O, and N_2 TONs as a function of NO pressure with a fixed CO pressure of 8 Torr at 623 K and 528 K over Rh(110).

N_2O, and N_2 formation over both Rh(110) and Rh(111) are compared. By our estimation, the experimental error in the E_a is about ±2 kcal/mol.

The effect of CO pressure on the NO–CO reaction rate over Rh(110) at two different temperatures (528 K and 623 K) is shown in Fig. 3. The NO pressure was kept constant at 8 Torr and the CO pressure was varied from 2 to 40 Torr. Within experimental error, the CO_2, N_2O, and N_2 TONs are invariant with CO pressure over the CO pressure range examined; that is, the NO–CO reaction has an apparent zero-order dependence on the CO pressure. A similar experiment was performed to obtain the NO reaction order. Figure 4 shows the reaction rate data obtained with the CO pressure held constant at 8 Torr and the NO pressure varied from 1 to 40 Torr at two different temperatures of 528 K and 623 K. At the lower temperature of 528 K, the reaction rate is invariant with NO pressure for all three reaction products. However, at 623 K there is a distinct deviation from zero order dependence for NO partial pressures of less than 10 Torr. While both the CO_2 and the N_2 rates are higher at lower pressure (negative order in NO), the N_2O formation rate at 623 K is significantly lower (positive order in NO) at the lower NO pressures. Thus, the selectivity of the reaction for N_2O formation is also markedly lower at low NO partial pressures. We will return to this point below (Fig. 6).

For purposes of direct comparison, we remeasured the NO pressure dependence on Rh(111) at 623 K, CO pressure of 8 Torr, and NO pressures varying from 1 to 40 Torr. The results, shown in Fig. 5, are very similar to those measured by Belton and Schmieg (4). In both cases, the reaction is found to be essentially insensitive to changes in NO pressure under these conditions; zero order within our experimental uncertainty (±0.2). In agreement with the Belton and Schmieg previous findings, we

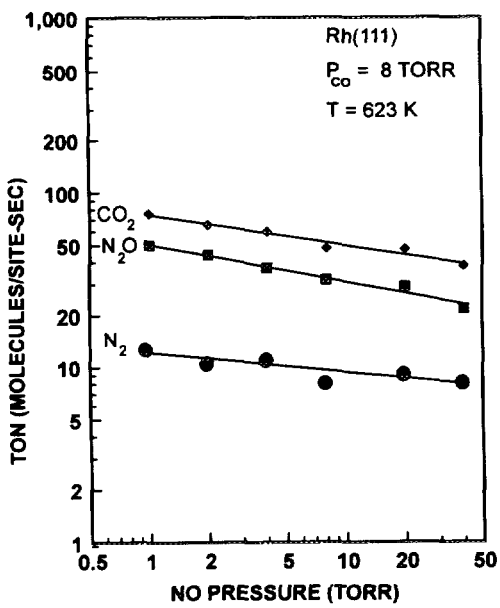

FIG. 5. The CO_2, N_2O, and N_2 TONs as a function of NO pressure with a fixed CO pressure of 8 Torr at 623 K over Rh(111).

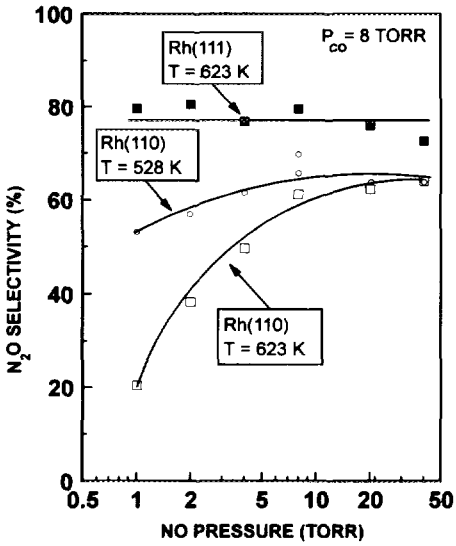

FIG. 6. N_2O selectivity plotted as a function of NO partial pressure at a fixed CO pressure of 8 Torr and at a temperature of either 623 K on Rh(111) (solid squares) and Rh(110) (open squares) or at 528 K on Rh(110) (open circles).

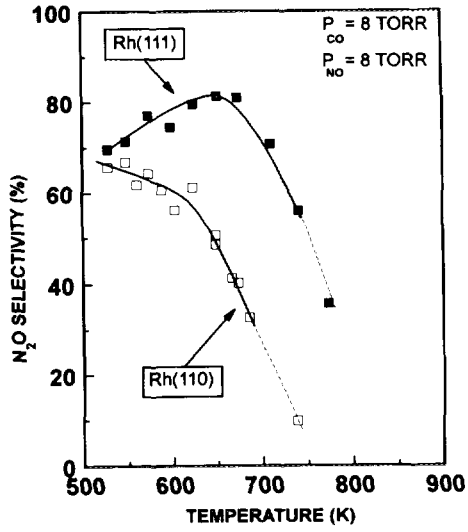

FIG. 7. Effect of temperature on N_2O selectivity over Rh(110) (open squares) and Rh(111) (solid squares) for a reactant mixture, P_{CO}/P_{NO} = 8/8. Conversion of NO was kept below 30% except for the data points connected by dashed lines (see text).

also found that over Rh(111) the NO–CO reaction is zero order in CO pressure. For brevity, the CO pressure-dependent reaction data are not shown here.

3.2. N_2O Selectivity

In this section, we will examine the effect of a number of experimental variables on the selectivity of the NO–CO reaction for the formation of the two nitrogen containing products, N_2 and N_2O. By convention (4, 11–17), in the following we report N_2O selectivity, S^{N_2O}, as [mol N_2O]/[mol N_2O + mol N_2]. Figure 6 compares Rh(110) and Rh(111) with regard to the effect of NO pressure on N_2O selectivity at a constant CO pressure of 8 Torr. For Rh(111) at 623 K, we observe no change in S^{N_2O} even for the lowest NO pressure of 1 Torr. This result is in very good agreement with previous results on Rh(111) (4) and those obtained on a highly loaded (5 wt%) Rh/SiO_2 catalyst (11). There is little sensitivity of the N_2O selectivity to NO pressure on Rh(110) at 528 K. However, we observe a marked decrease in the N_2O selectivity on Rh(110) at NO partial pressures below about 10 Torr for a reaction temperature of 623 K.

Before proceeding, we should note that all of the data in Figs. 1–6 were taken at temperatures between 573 K to 698 K with a NO conversion of less than 15%. This temperature/conversion regime represents the parameter space where we can very accurately determine the specific rates of the reaction. However, because it has been reported that N_2O selectivity falls dramatically at high temperatures and/or high NO conversions (12–17), we decided to explore the high temperature/conversion regime. *Although we cannot accurately determine the absolute reaction rates, we can still accurately measure the N_2O selectivity.*

The effect of temperature on selectivity is addressed more completely in Figs. 7 and 8, where a direct comparison between results on Rh(110) and Rh(111) is made. Specifically, we show the effect of temperature on N_2O selectivity using two different gas mixtures: 8 Torr NO/

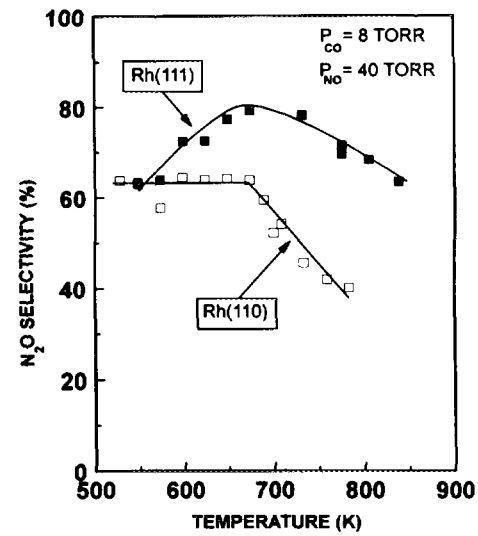

FIG. 8. Effect of temperature on N_2O selectivity over Rh(110) (open squares) and Rh(111) (solid squares) for a reactant mixture, P_{CO}/P_{NO} = 8/40. Conversion of NO was kept below 30%.

8 Torr CO (8/8) (Fig. 7) and 40 Torr NO/8 Torr CO (40/8) (Fig. 8). To separate as much as possible the effects of temperature and conversion, NO conversions were kept below 30%, with the exception of the two data points in Fig. 7 connected by dashed lines (see below). For Rh(110) (Fig. 7, 8/8) at temperatures below about 650 K, the selectivity toward N_2O falls slowly from about 70 to 60% as the temperature is changed from 575 K to 650 K. However, if the NO pressure is raised to 40 Torr (Fig. 8, 40/8) then the N_2O selectivity is insensitive to reaction temperature all the way up to 700 K. For either gas mixture (8/8 or 40/8) over Rh(110) at elevated temperatures (above 650 K, 8/8, and 700 K, 40/8), the N_2O selectivity is a strong function of temperature and this temperature-dependent selectivity is also a strong function of the reactant mixture employed. Once again, contrasting behavior was observed on Rh(111) as illustrated in Figs. 7 and 8. On this surface, N_2O selectivity actually increases slightly (from 70 to 80% for an 8/8 mixture, Fig. 7, and from 60 to 80% for NO/CO ratios of 40/8, Fig. 8) with temperature below 680 K. As with Rh(110), still higher temperatures led to a decrease in selectivity for N_2O. More importantly, however, is the fact that under all conditions studied here, the (111) surface shows a much stronger tendency to form N_2O and a much weaker selectivity dependence on either temperature or NO pressure. For example, note that even at 775 K, selectivity was still about 35% for Rh(111), whereas it was only 10% at the lower temperature of 740 K on Rh(110). On both surfaces, the decrease in selectivity at high temperatures was more gradual at the higher NO partial pressure of 40 Torr.

In Fig. 7, the data points obtained at the highest temperature for each surface are connected by a dashed line. This is to indicate the fact that these selectivity results were obtained at NO conversions significantly greater than 30%. In fact, when these reactions were run, it became impossible to control the temperature of the sample through resistive heating. When this occurred, the power supply controlling the sample temperature was turned off although the crystal temperatures remained at the values shown in the figure (Rh(110), 745 K; Rh(111), 775 K) for some time, and then began to fall. We believe that this behavior is analogous to the phenomenon of "light-off" that is observed in supported catalysts and occurs due to a change from solely kinetically limited reaction to a regime where heat and mass transfer effects become significant.

Figure 9 addresses the effect of NO conversion on N_2O selectivity at a constant temperature of 648 K. We observe little, if any change in selectivity on Rh(111) up to NO conversions as high as 87%. This result agrees with the previous work of Hecker and Bell (11), who measured essentially a constant N_2O selectivity of 80% for NO conversions below 90%. For low NO conversions (<50%) on Rh(110) at 648 K, the N_2O selectivity was found to be

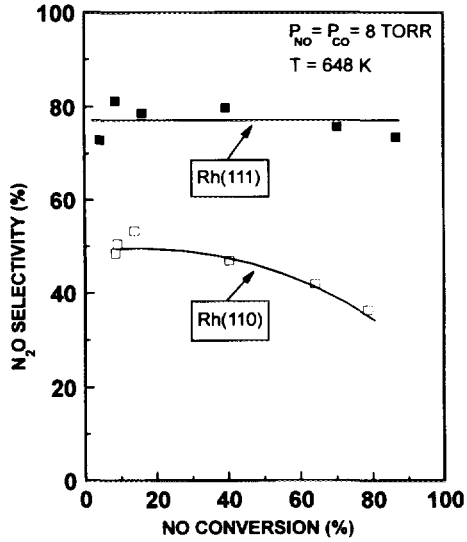

FIG. 9. Effect of NO conversion on N_2O selectivity at 648 K over Rh(110) (open squares) and Rh(111) (solid squares). Note that while on Rh(111) there is no significant change in selectivity even at high NO conversion, the selectivity shows a considerable dependence on conversion over Rh(110).

50% (Fig. 9), and it decreased somewhat at higher NO conversions. Note that since our measurements of selectivity versus conversion are made in a batch reactor, the measured selectivity at high conversions is in fact the integrated selectivity over all conversions to that point. As such, for an NO conversion of 80% on Rh(110), the actual N_2O selectivity at the time when the last NO molecules are being reacted must be quite low, probably approaching 0%.

3.3. Postreaction XPS Analysis

In a recent paper authored by Ng *et al.* (5), it was concluded that N_2O selectivity on Rh is a strong function of NO surface coverages during reaction. Therefore, it was reasonable to assume that the different selectivities we observed on Rh(110) and Rh(111) might be a direct result of differing steady-state concentrations of adsorbed surface species (notably NO) during reaction. One way to indirectly assess the state of the reactive surface is to perform a UHV surface spectroscopic measurement *ex situ* after reaction (24). In this case, we chose XPS because it can clearly distinguish between adsorbed nitrogen present as either molecular NO or as N atoms formed by NO dissociation during reaction (7, 25). Figure 10 shows the N(1s) region of XPS spectra taken after NO–CO reaction over both Rh(110) and Rh(111) at 528 K and NO and CO partial pressures of 8 Torr each. After the reactions were run, the samples were cooled in the reactant gases, freezing out the reaction, and then the reactor was evacuated

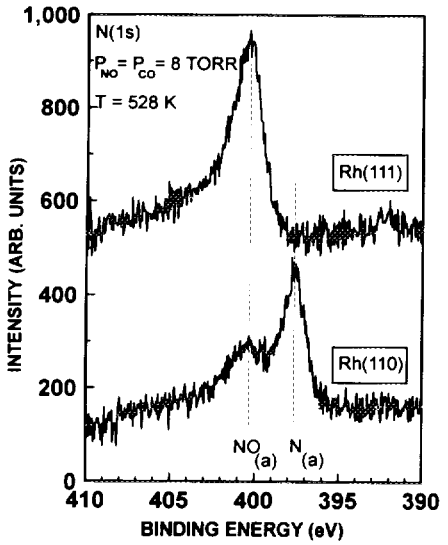

FIG. 10. N(1s) XPS spectra obtained after NO–CO reaction at 500 K in 8 Torr of each reactant. The crystals were cooled in the gas mixture after reaction, products analyzed by GC, and the gas mixture pumped out of the reactor prior to introduction into the UHV surface analysis chamber.

and the samples transferred to the UHV chamber for XPS analysis. For Rh(111), the spectrum shows only a single N(1s) feature with a binding energy near 400.3 eV due to adsorbed NO. In contrast, the NO N(1s) feature on Rh(110), while present, is significantly smaller than another N(1s) feature at lower binding energy, 397.6 eV, due to adsorbed N atoms.

IV. DISCUSSION

In the following, we discuss first the proposed reaction mechanism for the NO–CO reaction on Rh metal catalysts. This mechanistic picture, with its corresponding identification of possible rate-limiting elementary steps, will be used to understand the comparative reaction kinetics of the two single crystal substrates, Rh(110) and Rh(111), studied here. We follow this with a consideration of the differences observed in the product distribution for reaction on these two surfaces. Finally, we compare the present results with those published previously for single crystal and supported Rh metal and discuss the implications of the present results for understanding the behavior of more complicated supported catalyst systems.

4.1. Previously Proposed NO–CO Reaction Mechanisms

Several different mechanisms for the NO–CO reaction (11, 12, 16, 26–29) have been put forth over the years. However, new information regarding elementary steps on the close-packed (111) Rh surface (30–33) that sheds new light on the reaction mechanism has been obtained. In particular, it had been proposed previously (27) that a surface reaction between adsorbed NO and N atoms can provide an important channel for N_2 formation during steady-state reaction according to

$$NO(ad) + N(ad) \rightarrow N_2(g) + O(ad) + S, \quad [2]$$

where S represents a site for adsorption and/or reaction on the catalyst surface. This suggestion was based, in large part, on an interpretation of NO TPD results (8a, 19, 33–35) that now appears to have been unwarranted (32, 36). As such, the important elementary reactions were recently proposed to be (4, 5, 36)

$$CO(g) + S \Leftrightarrow CO(ad) \quad [3]$$

$$NO(g) + S \Leftrightarrow NO(ad) \quad [4]$$

$$NO(ad) + S \rightarrow N(ad) + O(ad) \quad [5]$$

$$CO(ad) + O(ad) \rightarrow CO_2(g) + 2S \quad [6]$$

$$NO(ad) + N(ad) \rightarrow N_2O(g) + 2S \quad [7]$$

$$N(ad) + N(ad) \rightarrow N_2(g) + 2S. \quad [8]$$

In this model, N_2O selectivity will depend on the relative rates of reactions [7] and [8]. These, in turn, are dependent on the relative surface coverages of NO and N. In recent reports (4, 5, 36), it was concluded that the rate and selectivity are controlled, in large part, by the NO adsorption/desorption equilibrium. Certainly NO coverages are dependent on this equilibrium. In addition, NO dissociation rates and therefore N atom coverages are strongly NO coverage-dependent as well (7, 9, 19, 33, 34, 37). Furthermore, measurements of the rate of step [8], N atom recombination to give N_2, gave values at relatively high N-atom coverages that were significantly higher than steady-state rates for the overall NO–CO reaction (31). This, therefore, led to speculation that NO dissociation, step [5], limits the rate of the NO–CO reaction (4, 5, 31, 36), an idea that had been proposed previously (29). Again, the rate of this latter reaction, step [5], is strongly dependent on the NO coverages and, therefore, the NO adsorption/desorption equilibrium.

We will use of the above-described reaction model to rationalize the comparative behavior of the two single crystal surfaces studied here. As discussed below, much of the data we obtained in the present study supports the conclusion that the NO adsorption/desorption equilibrium determines, in large part, the rate and selectivity of the NO–CO reaction.

It should be noted that in the mechanism shown above, surface sites for adsorption and reaction (denoted as S) are not distinguished for simplicity. There is ample evi-

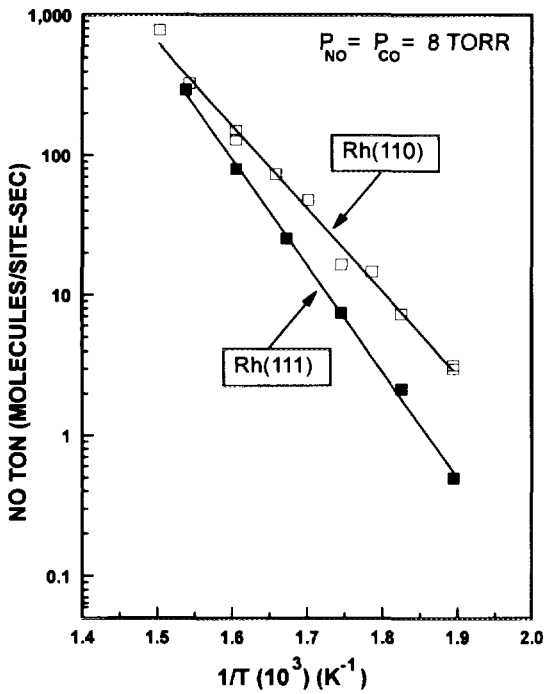

FIG. 11. Arrhenius plot of the rate of NO loss over Rh(110) (open squares) and Rh(111) (solid squares). NO TONs are calculated from N_2 and N_2O values reported in Figs. 1 and 2 based on the stoichiometry of the reaction [NO loss = 2(N_2 + N_2O formed)].

dence in the literature that, for example, adsorbed molecules may prefer different surface metal atom coordination geometries and therefore different binding sites that do adsorbed atomic species, and even binding sites below the first metal surface plane may be important for adsorbed atoms as has been suggested recently for N(ad) on Rh(110) (22). We raise this issue because it has, in fact, been proposed that NO and N atoms were not in direct competition for adsorption sites based on preliminary modeling of kinetic data obtained on Rh(111) (4) and more recently on experimental measurements (32).

4.2. NO–CO Reaction Kinetics on Rh(110) and Rh(111)

4.2.1. Rates of Reaction and Apparent Activation Energies

A direct comparison of overall NO–CO reaction rates is made in Fig. 11, where the rates of NO consumption obtained on both Rh(110) and Rh(111) are plotted. NO consumption represents the best relative measure of overall activity because it does not depend on the selectivity of the reaction (see Eq. [1] above). In this figure, we have calculated the NO reaction rates from the N_2 and N_2O turnover numbers using the stoichiometry of the reaction shown in Eq. [1]. Because the reactions were run at low conversions it is too difficult to measure small changes in the NO signal in the gas chromatograph. It should be kept in mind that we have normalized the rates on Rh(110) to the total number of metal atoms in the rows *and* troughs on this corregated surface. Despite this liberal estimate of reaction sites, the rate on Rh(110) over the temperature range studied here is as much as 6.3× higher than that obtained on Rh(111), and the reaction proceeds with a significantly lower apparent activation energy (27.2 vs 34.8 kcal/mol).

If one takes the view that NO dissociation limits the rate of reaction (4, 5, 31, 36) (see Section 4.1), it is tempting to simply attribute the differences in rates and apparent activation energies on the two single crystal surfaces to inherent variations in the kinetics of NO dissociation, Step [5], with surface structure. It is well recognized that, at least in low total adsorbate coverage ranges, the dissociation of small molecules on metals (6), and specifically NO on Rh (7–9), is generally faster and requires lower activation energies on rougher surfaces, such as the (110), relative to smooth surfaces (e.g., (111)). However at high surface NO coverages, the structure dependence of NO dissociation rates may not be as important as at low coverage. We say this because at high NO coverages the NO dissociation rates are dominated by the chemically modifying influence of the coadsorbates themselves, as well as the lower overall availability of dissociation sites (32, 33). Because of the NO coverage-dependent effects, the quantitative differences in overall rates and apparent activation energies observed in the present study can*not* be confidently rationalized based on low coverage estimates of NO dissociation rates. For the NO–CO reaction, many of the individual elementary reaction steps can and do have very similar reaction rates *under the conditions of temperature and pressure* used in the present experiments. Because of this fact, intuitively simple arguments should be used with caution (this should be kept in mind in all of the discussion to follow). Kinetic modeling, planned for the near future, should help to identify the most likely reaction step(s) whose rate(s) are significantly different on the two single crystal surfaces. However, important clues to the variable behavior are contained in the pressure dependence of reaction that we discuss next.

4.2.2. Pressure Dependence of the Reaction Rates and N_2O Selectivities

For Rh(111), under virtually all experimental conditions where we can accurately measure TONs in this (Fig. 5) and a previous (4) study, the reaction rates for the formation of any of the products (CO_2, N_2, and N_2O) show little if any dependence (approximately zero order) on the partial pressure of either reactant. This means, of course, that the N_2O selectivity is also independent of reactant partial pressures (e.g., as shown in Fig. 6). Similarly,

we found that the reaction was zero order in CO partial pressure over Rh(110) at an NO pressure of 8 Torr (Fig. 3). However, the dependence of the reaction rates on NO partial pressure for Rh(110) shown in Fig. 4, and correspondingly, the N_2O selectivity (Fig. 6) are considerably different below and above 600 K. Similarly, a comparison of the results shown in Figs. 7 and 8 demonstrates that N_2O selectivities become dependent on NO pressure on Rh(111) at temperatures above 700 K. As such, we consider these two reaction regimes separately.

4.2.2.1. Low-temperature (<600 K) behavior. We first consider the reaction regime that is characterized by kinetics and N_2O selectivities that are essentially zero order in the partial pressures of both reactants. This regime was discussed at some length in recent papers by Belton and Schmieg (4) and Ng *et al.* (5), so we only briefly summarize the main conclusions here. In these previous papers, it was argued that the remarkable insensitivity of the reaction rates and selectivities over Rh(111) (4) and $Pt_{10}Rh_{90}(111)$ (5) catalysts to virtually all experimentally accessible variables was most simply and most plausibly rationalized in the following way. For the reasons discussed above in Section 4.1, the two nitrogen-containing products, N_2 and N_2O, are assumed to form competitively from the separate reaction Steps [7] and [8], and *not* via a common surface intermediate N_2O-like species (both reactions [2] and [7] occurring simultaneously). Then, N_2O selectivities do not change with reaction conditions because the surface coverages of the reactants of steps [7] and [8], NO and N atoms, are not changing. This, of course, implies that the surface coverages of CO and O atoms are not likely changing either although their steady-state concentrations are expected to be small due to the fact that the surface reaction between adsorbed CO and O atoms is so rapid. For example, steady-state rates of CO_2 formation from the CO + O_2 reaction on Rh single crystal catalysts (10, 27) are at least an order of magnitude higher than those reported here for the NO–CO reaction shown in Figs. 1 and 2.

Because the temperature and pressure dependencies of the adsorption, desorption, and decomposition rates for NO (and CO for that matter) are considerable, the lack of variation in the surface coverages must then result from the fact that the surface is essentially saturated at the sites where NO (and CO) initially adsorb for our reaction conditions. Only at much lower total or partial pressures than we are able to access in these experiments (or at much higher temperatures, see below) would the N_2O selectivities be expected to vary with temperature and/or reactant pressures. In fact, studies of the NO–CO reaction over Rh carried out in UHV at pressures below 10^{-3} Torr all show the formation of N_2 as the only N-containing product (19–22). At the higher total pressures used in this study, running reactions at significantly higher temperatures (>600 K on Rh(110), for example) will result in changing surface coverages and correspondingly in changing kinetics and N_2O selectivities as demonstrated in the next section.

4.2.2.2. High-temperature (>600 K) behavior. At temperatures above 600 K over Rh(110), both the reaction rates (Fig. 4), and the N_2O selectivities (Fig. 6) depend on NO partial pressure. Furthermore, a comparison of the results shown in Figs. 7 and 8 demonstrates that Rh(111) shows similar NO pressure dependence above 700 K. For both surfaces, the selectivity for N_2O decreases with decreasing NO pressure. Ng *et al.* recently proposed that changing surface coverages of NO and N (and possibly CO and O as well) could account for similar results obtained for the NO–CO reaction on a $Pt_{10}Rh_{90}(111)$ alloy catalyst (5). Notably, the higher temperatures lead to lower steady-state concentrations of adsorbed NO. In the mechanism proposed above in Section 4.1, it is suggested that the rate of NO dissociation (step [5]) limits the overall rate of reaction and, in turn, determines the N_2O selectivity. Therefore, lower NO coverages that occur at higher temperatures should lead to more rapid NO dissociation, higher N atom coverages, and a correspondingly higher propensity for N_2 formation relative to N_2O (lower N_2O selectivities). This is most clearly indicated by the fact that an increase in NO pressure at these high temperatures results in an increase in the N_2O selectivity for both Rh surfaces (compare Figs. 7 and 8) because, of course, higher NO pressures will lead to higher NO coverages *as long as the NO surface coverage is sufficiently far away from saturation.*

It is useful to discuss the results shown in Fig. 9 at this point as they lend further support to the mechanistic arguments that we have been making. In the figure, it is demonstrated that the N_2O selectivity drops significantly on Rh(110) at higher NO conversions for reaction at 650 K. (While Rh(111) shows no sensitivity to NO conversion at this temperature (see Section 4.3 below), we believe (38) that just such a sensitivity would be observed for temperatures above 700 K on this surface.) At sufficiently high NO conversions (>50%), NO partial pressures will be significantly lower, thereby leading to a drop in the surface coverage of NO, more facile NO dissociation, and, therefore, lower N_2O selectivities.

The results shown in Fig. 4 demonstrate that, at temperatures above 600 K on Rh(110), the N_2O selectivity decreases with decreasing NO pressure. In addition, the rate of CO_2 formation and NO consumption is increasing as the NO pressure is decreased (we calculate a 25% increase in NO consumption between 10 and 1 Torr). This apparently negative order region is suggestive that the NO coverage on Rh(110) is changing at the lowest NO pressures and highest reaction temperatures. We suspect

that similar results would be observed on Rh(111) above temperatures of 700 K or at NO pressures below 1 Torr. Unfortunately, we were not able to accurately measure the pressure dependence of the reaction rates on Rh(111) under these conditions due to limitations of the reactor and GC detection. In any case, the result on Rh(110) can again be rationalized within the model that the NO dissociation rate (step [5]) limits the overall reaction rate and that this rate is, in turn, slower at higher NO coverages.

4.2.3. Summary: NO–CO Reaction Kinetics

In summary, the kinetic results obtained on both Rh surfaces can all be readily accounted for with the model discussed above in Section 4.1, with the important assumption that NO dissociation (step [5]) is the critical step (probably rate-limiting) under the high-pressure reaction conditions used in these experiments. The mechanistic arguments that we make also rely on the important fact that NO dissociation rates are suppressed at high NO surface coverages (7, 9, 33, 34, 37). Therefore, the NO adsorption/desorption equilibrium is a primary determining factor of N_2O selectivities for both Rh(111) and Rh(110) surfaces. (The variable behavior of these two surfaces with respect to selectivity and its sensitivity to reaction conditions is discussed below in Section 4.3.) Before leaving this section, we would like to emphasize again that this mechanistic picture should be tested with mathematical modeling that uses, as much as possible, measured kinetics of the elementary steps in order to verify that it can *quantitatively* describe the overall reaction kinetics observed here.

4.3. Effect of Surface Structure on N_2O Selectivity

In this section, we discuss possible explanations for the significantly different N_2O selectivities observed on the two single crystal catalysts used in this study, Rh(110) and Rh(111). The fact that the selectivity for N_2O as measured over Rh(111) and Rh(110) shows quite different sensitivities to NO pressure (Fig. 6), reaction temperature (Figs. 7 and 8), and NO conversion (Fig. 9) will also be considered. At this point in time our understanding of the rates of some elementary steps is too limited to allow us to make definitive statements as to the details of how the surface structure effects the N_2O selectivity. Based on the discussion in Sections 4.1 and 4.2, we proceed under the assumption that the much greater tendency of Rh(110) to form N_2 (much less selective for N_2O) than Rh(111) results from differences in the relative rates of reactions [7] and [8] (Section 4.1). In addition, until we have obtained further information as to the N atom recombination rates and N_2O formation rates on Rh(110), we must assume that the *rate constants* for these reactions are similar on the two different surfaces. Within this framework of assumptions, the differences in N_2O selectivity must arise from different steady-state *coverages* of NO and N atoms on these two surfaces during high-pressure reaction. In fact, we have some fairly direct evidence in support of this assumption from the XPS results shown in Fig. 10. Although we do not believe that these measurements directly determine the steady-state coverages, we argue that they do reflect the fact that reaction on Rh(110) occurs on a surface that contains significantly higher concentrations of N atoms than does reaction on Rh(111). The main question that we wish to address in this section is what could give rise to these differences in steady-state surface coverages. In order to answer this question, we must address the selectivity in two distinctly different kinetic regimes: low temperatures where the reaction for both surfaces is zero order in NO, and at higher temperatures where the (111) surface is zero order but (110) shows a negative order in NO.

4.3.1. Selectivity Differences at Low (<600 K) Reaction Temperature

For reaction at low temperatures (where both surfaces are zero order in NO pressure), the simplest argument one could make to account for larger steady-state coverages of N-atoms on Rh(110) versus Rh(111) would be an *intrinsically* faster rate of NO dissociation on the former surface. That is, there are certain more favorable surface geometric structures and/or electronic properties of the rougher (110) surface that give rise to a more rapid rate of NO dissociation. There is certainly a significant amount of lore in the surface science literature that the dissociation of molecules occurs more readily on atomically rough surfaces like the fcc(110) than on smooth surfaces such as close-packed fcc(111) (6). Recent work (7–9) suggests just such a propensity for NO dissociation on Rh. Furthermore, results from TPD experiments following the adsorption of saturation coverages of NO on a number of single crystal surfaces indicate that the relative proportion of N_2 versus NO desorption is somewhat higher on Rh(110) (22, 35) than on the (100) (34) or (111) (33) surfaces of Rh. However, these TPD results do not provide direct evidence for an *intrinsically* faster NO dissociation any more than the steady-state kinetics that we present here. Indeed, during TPD from all three Rh surfaces using low coverages of NO, all of the adsorbed NO undergoes complete dissociation with N_2 being the only N-containing desorption product. In this low coverage limit, NO dissociation is a very rapid reaction step that would probably not be rate limiting to the NO–CO reaction. Therefore, under reaction conditions where NO coverages are very low, we would not expect that the NO–CO reaction rate

to be particularly sensitive to the structural differences in the NO dissociation rates. However, in the 1–100 Torr pressure range NO coverages are likely near saturation and thus dissociation rates in the low coverage limit may in fact be misleading.

A second possible explanation that one can make as to why the (110) surface has higher steady state N-atom coverages focuses on the "self-inhibition" of NO for dissociation. It has been shown that adsorbed NO strongly inhibits NO dissociation on Rh(111) and Rh(100) surfaces (7, 33, 34). It is likely that this is true to some extent on Rh(110) as well, but because of the more open structure of the (110) surface, it seems reasonable that adsorbed NO may not as strongly inhibit NO dissociation. By our way of thinking, this is basically a steric argument whereby the large surface atom spacing (between the rows) gives the NO molecules more room within which to lie down (presumably into the troughs) and thus dissociate. Under this scenario we explain our results in the following manner. In the low temperature region (<600 K), the reaction is very close to zero order in NO pressure, so it is clear that both surfaces are essentially saturated with NO; therefore, the reaction is "fully inhibited" (*to the extent possible on that surface*) by adsorbed NO. Within the *zero order in NO* domain, the (110) surface produces more N_2 than will the (111) surface due primarily to due less steric hindrance for NO dissociation at saturation NO coverages. Thus, for saturation NO, the NO dissociation rate is higher on (110) and the steady-state N atom coverages are correspondingly higher.

The third possible explanation for higher steady-state N-atom coverages on Rh(110) centers around the basic competition of NO and N for sites on the Rh surfaces. In recent work (32), we found that adsorbed N-atoms had very little effect on either the amount of NO that can adsorb on Rh(111) or on the rate that NO desorbs from that surface. We suspect that the story is somewhat different for the (110) surface. It appears that N-atoms have a strong tendency to block NO adsorption on the (110) surface. We base this conclusion on the XPS data shown in Fig. 10. Recall that prior to introduction into the XPS analysis chamber, the surface whose XPS spectrum is shown in Fig. 10, was sitting at 300 K in 8 Torr of NO and CO. Clearly, the surface would be saturated in NO (no CO is observed) after such a treatment; therefore, we contend that the reason so little NO is observed with XPS is that the adsorbed N atoms are blocking NO adsorption on this surface. We feel that this effect may be most important in leading to lower NO coverages and likewise faster NO dissociation on the more open surface. Our current thinking is that deposition of *N* atoms on the (110) surface tends to block further NO adsorption on that surface, thus enhancing the NO dissociation rate by lifting some of the NO inhibition of NO dissociation. As such, we are exploring the interactions of NO and N on the Rh(110) surface in a manner similar to that previously studied on the (111) surface (32). With our current understanding of the relative rates of elementary steps, any of the above three arguments could explain the observed differences in Rh(111) and Rh(110) kinetics in the zero-order (in NO) domain where NO coverages are saturated.

4.3.2. Selectivity Differences at Higher Temperature

The preceding paragraphs gave plausible explanations for the structure sensitivity in the low temperature, NO pressure independent regime; however, we must still explain why the two surfaces show different NO pressure dependencies at intermediate temperatures (600 K < T < 700 K). Recall that changing the NO pressure at 625 K on the (111) surface does not lead to significant changes in the selectivity for N_2O, while on the (110) surface the N_2O selectivity falls sharply (Fig. 6) for NO pressures below 10 Torr. Similarly, Fig. 7 demonstrates that N_2O selectivities are being dramatically lowered with increasing temperature (600 K < T < 700 K) on Rh(110), while the selectivity over the (111) surface does not change. It is clear that the primary effect of lowering the NO pressure must be to lower the surface NO coverage, which in turn lowers the N_2O production rate (Fig. 4) over Rh(110). We assume that raising the temperature has primarily the same effect; however, this may not be true since different elementary steps have different activation energies. Therefore, we will focus on the NO pressure-dependent data by asking why the reaction remains approximately zero order over Rh(111) in this same temperature/pressure regime for which it is negative order (for N_2 and CO_2) over Rh(110). Clearly, lowering the NO pressure at a fixed temperature must affect primarily the NO adsorption/desorption equilibrium. Based on TPD results from *clean* Rh single crystals (22, 33–35), there does not appear to be any significant differences in the desorption rates of NO from the (100), (111), and (110) surfaces. Therefore, we are left to conclude that it is the NO adsorption part of the equilibrium that is most different on the two surfaces. We suggest that since NO adsorbs via a mobile precursor it is able to sample more adsorption sites when adsorbing on the close packed (111) surface than when adsorbing on the atomically rough (110) surface. Sampling more sites during the adsorption process keeps the NO sticking coefficient high (around 0.5 at low coverages on both surfaces) to a much higher NO coverage on (111) than on Rh(110). As a result we would expect higher steady-state NO coverages on Rh(111) than on Rh(110) under the same conditions of NO pressure and surface temperature. The result of these subtle differences in NO sticking would be that different NO pressures would be required (at a fixed temperature) to saturate the two differ-

ent surfaces. Thus, NO dissociation, which slows down as the surface nears saturation (we estimate about a factor of 3 difference in the dissociation rate for between 0.3 and 0.75 ML of NO on Rh(111) (32)), would be faster on the (110) surface which has a lower NO coverage.

A second explanation as to why the two surfaces show different NO pressure dependencies at intermediate temperatures (600 K $< T <$ 700 K) goes as follows. Given that TPD data show a strong tendency for adsorbed NO to inhibit NO dissociation (presumably by blocking needed dissociation sites), it may be true that the functional dependence of the NO dissociation rate on NO coverage varies markedly on the two different surfaces. We would suspect that over Rh(111) the dissociation rate is not very sensitive to small changes in NO coverage for NO coverages near saturation. Thus for Rh(111), rather large changes (say 30% for the sake of this discussion) may be required in order to get a significant change in the NO dissociation rate and thereby affecting the overall reaction rate or selectivity. If on the other hand, NO dissociation on the (110) surface is very sensitive to small NO coverage changes, then dropping the NO coverage by the same 30% (arbitrarily chosen) would have a larger (relative to (111)) effect on NO dissociation. Thus, the (110) surface would show selectivity differences for much smaller surface NO coverage changes than does Rh(111) because NO dissociation on (110) is more NO coverage sensitive.

4.3.3. Summary: Differences in Selectivity

What should be clear from the above discussion is that although the N_2O selectivity differences we observe in this study are quite dramatic and that the differences can be readily understood in terms of different steady-state coverages on NO and N atoms on the two surfaces, the underlying causes of these differences may be quite subtle. It should also be evident that these subtle differences can be understood only by making additional detailed measurements of the NO adsorption (including sticking coefficients), desorption, and dissociation rates. In particular we need these measurements to be made in the presence of coadsorbed N-atoms. Indeed, one of the most useful aspects of this study is that it allowed us to very specifically target several areas for which the current information regarding elementary steps is incomplete. It is our observation that despite the relatively large number of papers on the interactions of NO with Rh surfaces, much of that work is either in a coverage or temperature regime that is not particularly germane to reactions in the 10-Torr pressure range. Furthermore at this point in time, our understanding of the reaction mechanism is too limited to make full use of some of the beautiful work done characterizing surface structures with LEED and/or adsorbate geometry with vibrational spectrocopies.

4.4. Implications for Supported Catalysts

There are a number of similarities in the behavior of these two single crystal catalysts and that observed for high surface area oxide-supported Rh catalysts (11–17). There are also a number of differences that seem to be evident between the behavior of the model and more practical materials. These will be described and discussed in this section in order to assess the general applicability of the mechanistic insights gained in the present study of model single crystal catalysts for understanding the reactivity of the practical supported catalysts systems. Before doing so, we remind the reader that there are clear differences in the reactor design in the two sets of studies (batch reactor in the single crystal studies and flow reactors for kinetic measurements of supported catalysts). As such, not all results are expected to be exactly comparable. For example, varying the space velocity in a flow reactor shifts the temperature at which products can be detected and, thus, kinetics studied over supported catalysts. Since in most cases, the TON's are not reported for supported catalysts, then direct comparisons of rates are not usually possible.

As was discussed at some length in a previous paper by Belton and Schmieg (4), the kinetic results (activation energy, pressure dependence, product distributions) obtained on Rh(111) are remarkably similar to those reported for a 5 wt% Rh/SiO_2 catalyst by Hecker and Bell (11). Of principle interest for the present study is the fact that both of these catalysts showed N_2O selectivities near 80% and that the selectivities were largely invariant with NO conversion. This behavior contrasts significantly with that observed for low-loaded Rh/Al_2O_3 materials where N_2O selectivities are generally lower and much more sensitive to NO conversion levels (12–17). The results we report here for the NO–CO reaction on Rh(110) (Fig. 9) are similar to the results obtained over low-loaded Rh/Al_2O_3 materials. The surfaces of small metal particles supported on oxide materials are known to be quite heterogeneous while larger particles tend to expose only a few (at most) of the lower surface energy planes (largely (111) for fcc metals) (39). Thus, a simple explanation for the different behavior of the various supported catalysts is that it arises from variations in surface crystallography. Indeed, the remarkable similarity in the results for a highly loaded silica-supported Rh catalyst (11) with those obtained here and previously (4) on Rh(111) suggest that the surfaces of these large Rh particles were predominantly (111)-oriented. We would not propose that the smaller metal particles of low-loaded Rh catalysts are completely modeled by the (110) surface (their surface structures are undoubtedly more complex), and, in fact, we find several differences for which we currently cannot completely account (see below). Still, we believe that the present study has pro-

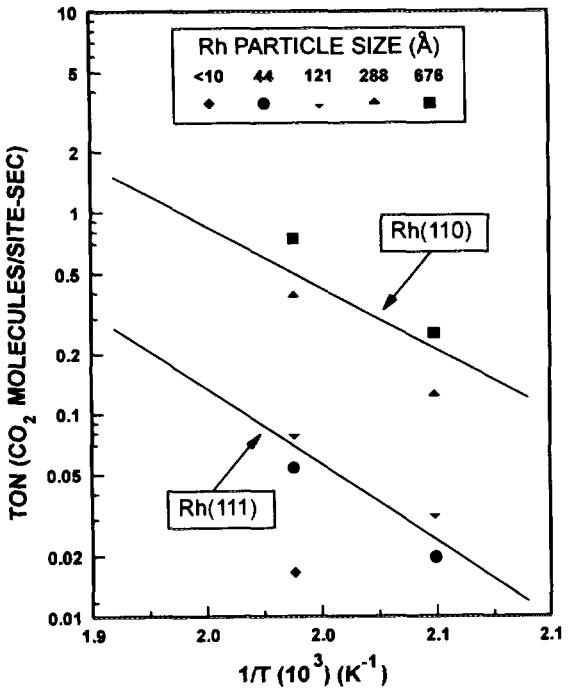

FIG. 12. A comparison of CO_2 TONs from the NO–CO reaction over Rh(110) (solid line extrapolated from Fig. 1), Rh(111) (solid line extrapolated from Fig. 2), and several Rh/Al_2O_3-supported catalysts with varying particle sizes (15) as indicated.

vided strong evidence that surface geometric structure is playing a crucial role in determining the reactivity and selectivity of supported Rh catalysts for the NO–CO reaction.

A more direct comparison between the present results and previous studies of supported Rh catalysts (15) is made in Fig. 12. A similar comparison (not shown) of the kinetics for the $CO–O_2$ reaction from the same supported Rh catalysts (15) with previously published measurements on single crystals (10, 27) shows that both supported and single crystal catalysts have nearly identical rates (per surface atom). In Fig. 12 it is demonstrated that both the absolute activities and the activation energies for CO_2 formation from the NO–CO reaction are very similar on the supported and single crystal catalysts. What is especially curious about this comparison, however, is that the catalysts with the *largest* Rh particles (>200 Å) appear to have (110)-like activities while catalysts with intermediate-sized particles (50–150 Å) show activities that are comparable to those we obtained on Rh(111). A recent study of the activity and selectivity of the *n*-butane hydrogenolysis reaction compared the behavior of a number of supported Rh catalysts with varying metal loadings with Rh(111), Rh(100), and Rh(110) single crystals (40). In this study, it was found that alumina- and silica-supported catalysts containing metal particles as small as 25 Å gave activities and selectivities that were comparable to the kinetics measured on the Rh(111) surface. These results are then, perhaps, consistent with the fact that catalysts with intermediate-sized Rh particles show (111)-like activity for the NO–CO reaction. However, this conclusion is clearly inconsistent with the results in Fig. 12 for the catalysts with the largest Rh particles as one expects the (111)-type behavior to dominate on these even larger Rh particles. One complicating factor that must be considered is that structural changes occur in the supported Rh catalysts depending on the gas phase composition and reaction temperature (40). For large particle (>60 Å) silica-supported Rh catalysts, a moderate temperature treatment in O_2 resulted in metastable surfaces that gave *n*-butane hydrogenolysis selectivities more comparable to those obtained from Rh(100) and Rh(110) surfaces (40). High temperature (773 K) H_2 reduction restored (111)-like selectivities. These results raise the intriguing possibility that surface species present during steady-state NO–CO reaction may themselves control the surface structure of Rh particles in oxide-supported catalysts. In fact, there have been several recent demonstrations that adsorbed N (and O) atoms can restructure Rh surfaces (22, 41, 42). Another important consideration, however, is the fact that Oh and Eickel (15) find only a small variation in the N_2O selectivity with particle size for catalysts with Rh particles > 100 Å. It would certainly be interesting to follow the sensitivity of this selectivity for supported catalysts with even smaller-sized Rh particles.

More generally, we believe that we have shown that the overall behavior of both model and realistic catalysts is similar. As such, we claim that the mechanistic arguments made here almost certainly apply to the supported catalysts. The primary conclusion of our kinetic studies is that the NO adsorption/desorption equilibrium plays a critical role in determining not only the overall rate of reaction, but the selectivity for the various nitrogen containing products as well. This is so because the surface is essentially saturated with adsorbed NO under moderate temperature and pressure conditions like those used in this study and because high coverages of NO have such a profound effect on the rate of NO dissociation.

V. CONCLUSIONS

CO and NO were reacted over both Rh(110) and Rh(111) surfaces in order to understand the effect of Rh surface structure on the activity and selectivity of Rh for NO reduction. Our results show that the NO–CO reaction is very sensitive to the Rh surface structure primarily with regard to the selectivity of the reaction for N_2O. With regard to activity, or specific rates, we find that both surfaces consume NO at similar rates, with reaction on the (110) surface taking place between 1.5 and 13× faster

than on Rh(111), depending on how you account for surface sites on the Rh(110) surface and at what temperature the comparison is made. Furthermore, we observed that the (110) surface consumes NO with a lower apparent E_a than does Rh(111) over the range of temperatures and pressures that we examined. In contrast to the sometimes similar activities of the (111) and (110) surfaces, these surfaces have very clear differences with regard to the selectivity of the reaction for N_2O formation. Qualitatively the (110) surface shows a much stronger tendency toward N_2 production than does the (111) surface. Whereas the (111) surface produces greater than 70% N_2O under almost all experimental conditions of this study, we observed selectivities as low as 8% for the (110) surface. At the present time, we do not have detailed modeling to account for these selectivity differences; however, based on our kinetic results, we feel confident that the differences in these two surface is related to the manner in which adsorbed NO inhibits the NO dissociation reaction. Available surface science results suggest that the NO desorption does not differ significantly on these two surfaces. However, NO dissociation that was less "inhibited" by coadsorbed NO on Rh(110) would lead to greater steady-state concentrations of adsorbed N atoms, thus providing more favorable conditions for N atom recombination relative to the NO + N atom reaction to make N_2O. With regard to supported catalysts, our results clearly demonstrate that particle size effects are a reasonable way of understanding the selectivity differences observed for catalysts with different Rh loading.

ACKNOWLEDGMENTS

CHFP thanks Kathy Taylor and Galen Fisher of GMR&D's Physical Chemistry Department for the opportunity to visit GMR&D and perform these experiments.

REFERENCES

1. Taylor, K. C., *Chemtech* **20,** 551 (1990).
2. Taylor, K. C., *Catal. Rev. Sci. Eng.* **35,** 457 (1993).
3. Calvert, J. G., Heywood, J. B., Sawyer, R. F., and Seinfeld, J. H., *Science* **261,** 37 (1993).
4. Belton, D. N., and Schmieg, S. J., *J. Catal.* **144,** 9 (1993).
5. Ng, K. Y. S., Belton, D. N., Schmieg, S. J., and Fisher, G. B., *J. Catal.* **146,** 394 (1994).
6. For example, see (a) Benziger, J. B., *Appl. Surf. Sci.* **6,** 105 (1980), and (b) Zaera, F., Gellman, A. J., and Somorjai, G. A., *Acct. Chem. Res.* **19,** 24 (1986).
7. DeLouise, L. A., and Winograd, N., *Surf. Sci.* **159,** 199 (1985).
8. (a) Hendrickx, H. A. C. M., and Nieuwenhuys, B. E., *Surf. Sci.* **175,** 185 (1986). (b) Hendrickx, H. A. C. M., Winkelman, A. M. E., and Nieuwenhuys, B. E., *Appl. Surf. Sci.* **27,** 458 (1987).
9. van Tol, M. F. H., and Nieuwenhuys, B. E., *Appl. Surf. Sci.* **67,** 188 (1993).
10. Peden, C. H. F., Goodman, D. W., Blair, D. S., Berlowitz, P. J., Fisher, G. B., and Oh, S. H., *J. Phys. Chem.* **92,** 1563 (1988).
11. Hecker, W. C., and Bell, A. T., *J. Catal.* **84,** 200 (1983).
12. Cho, B. K., Shanks, B. H., and Bailey, J. E., *J. Catal.* **115,** 486 (1989).
13. McCabe, R. W., and Wong, C., *J. Catal.* **121,** 422 (1990).
14. Oh, S. H., *J. Catal.* **124,** 477 (1990).
15. Oh, S. H., and Eickel, C. C., *J. Catal.* **128,** 526 (1991).
16. Cho, B. K., *J. Catal.* **131,** 74 (1991).
17. Cho, B. J., *J. Catal.* in press (1994).
18. Hendershot, R. E., and Hansen, R. S., *J. Catal.* **98,** 150 (1986).
19. Campbell, C. T., and White, J. M., *Appl. Surf. Sci.* **1,** 347 (1978).
20. Lintz, H.-G., and Weisker, T., *Appl. Surf. Sci.* **24,** 259 (1985).
21. Schwartz, S. B., Fisher, G. B., and Schmidt, L. D., *J. Phys. Chem.* **92,** 389 (1988).
22. Baraldi, A., Dhank, V. R., Comelli, G., Kiskinova, M., and Rosei, R., *Appl. Surf. Sci.* **68,** 395 (1993).
23. Fisher, G. B., and Schmieg, S. J., *J. Vac. Sci. Technol. A* **1,** 1064 (1983).
24. For example, see Peden, C. H. F., in "Surface Science of Catalysis: *In-Situ* Probes and Reaction Kinetics" (D. J. Dwyer and F. M. Hoffman, Eds.), p. 143. American Chemical Society, Washington, DC, 1992, and references therein.
25. Baird, R. J., Ku, R. C., and Wynblatt, P., *Surf. Sci.* **97,** 346 (1980).
26. Chin, A. A., and Bell, A. T., *J. Phys. Chem.* **87,** 3700 (1983).
27. Oh, S. H., Fisher, G. B., Carpenter, J. E., and Goodman, D. W., *J. Catal.* **100,** 360 (1986).
28. Cho, B., *J. Catal.* **138,** 255 (1992).
29. Hecker, W. C., and Bell, A. T., *J. Catal.* **85,** 389 (1984).
30. Belton, D. N., and Schmieg, S. J., *J. Catal.* **138,** 70 (1992).
31. Belton, D. N., DiMaggio, C. L., and Ng, K. Y. S., *J. Catal.* **144,** 273 (1993).
32. Belton, D. N., DiMaggio, C. L., Schmeig, S. J., and Ng, K. Y. S. *J. Catal.*, in press (1995).
33. (a) Root, T. W., Schmidt, L. D., and Fisher, G. B., *Surf. Sci.* **134,** 30 (1983). (b) Root, T. W., Schmidt, L. D., and Fisher, G. B., *J. Chem. Phys.* **85,** 4679 (1986).
34. Ho, P., and White, J. M., *Surf. Sci.* **137,** 103 (1984).
35. Bowker, M., Guo, Q., and Joyner, R. W., *Surf. Sci.* **257,** 33 (1991).
36. Belton, D. N., Schmieg, S. J., Fisher, G. B., and Ng, K. Y. S., 40th National Symposium of the American Vacuum Society (November, 1993). [Abstract SS1-TuM1]
37. (a) Villarubia, J., and Ho, W., *J. Chem. Phys.* **87,** 750 (1987). (b) Whitman, L., and Ho, W., *J. Chem. Phys.* **89,** 762 (1988).
38. This proposal is supported by exactly this result obtained on a $Pt_{10}Rh_{90}(111)$ alloy catalyst (5). Notably, it was found in this study that the behavior of the alloy catalyst was simply a result of Rh(111) activity and that Pt merely diluted the Rh surface concentration (an inert site blocker).
39. van Hardeveld, R., and Hartog, *Surf. Sci.* **15,** (1969) 189.
40. Kalakkad, D., Anderson, S. L., Logan, A. D., Peña, J. Braunschweig, E. J., Peden, C. H. F., and Datye, A. K., *J. Phys. Chem.* **97,** 1437 (1993).
41. (a) Comelli, G., Dhanak, V. R., Kiskinova, M., Pangher, N., Paolucci, G., Prince, K. C., and Rosei, R., *Surf. Sci.* **260,** 7 (1992). (b) Lizzit, S., Comelli, G., Hofmann, Ph., Paolucci, G., Kiskinova, M., and Rosei, R., *Surf. Sci.* **276,** 144 (1992). (c) Comelli, G., Lizzit, S., Hofmann, Ph., Paolucci, G., Kiskinova, M., and Rosei, R., *Surf. Sci.* **277,** 31 (1992). (d) Morgante, A., Cvetko, D., Santoni, A., Prince, K. C., Dhanak, V. R., Comelli, G., and Kiskinova, M., *Surf. Sci.* **285,** 227 (1993). (e) Baraldi, A., Dhanak, V. R., Comelli, G., Prince, K. C., and Rosei, R., *Surf. Sci.* **293,** 246 (1993).
42. Voss, C., Gaussmann, A., and Kruse, N., *Appl. Surf. Sci.* **67,** 142 (1993).